

Pr²R: Information-Fused and Style-Aware Privacy-Preserving Replay for Lifelong Person Re-Identification

Mingyu Wang, Haojie Liu, Zhiyong Li, Wei Jiang

Abstract—Lifelong person re-identification (LReID) aims to incrementally accumulate knowledge across a sequence of tasks under domain shifts. Recently, replay-based methods have demonstrated strong effectiveness in LReID by rehearsing past samples stored in an auxiliary memory. However, storing historical exemplars raises concerns over data privacy. To avoid this, exemplar-free approaches attempt to match the distribution of past data without storing raw samples. Despite being privacy-friendly, these methods often suffer from performance degradation due to the forgetting of specific past knowledge representations. To this end, we propose to fuse information from sequential data into the pixel space in the replay memory, enabling Privacy-Preserving Replay (Pr²R). More specifically, by distilling the training characteristics of multiple real images into a single image, the fused samples undergo pixel-level changes. This not only protects the privacy of the original data but also makes the replay samples more representative for sequential tasks. During the style replay phase, we align the current domain to the previous one while simultaneously adapting the replay samples to match the style of the current domain. This dual-alignment strategy effectively mitigates both class-incremental challenges and forgetting caused by domain shifts. Extensive experiments on multiple benchmarks show that the proposed method significantly improves replay effectiveness while preserving data privacy. Specifically, Pr²R achieves 4% and 6% higher accuracy on sequential tasks compared to the current state-of-the-art and other replay-based methods, respectively.

Index Terms—Lifelong person Re-identification, Privacy Preserving, Information Fusion, Style Replay.

I. INTRODUCTION

PERSON re-identification (Re-ID) aims to retrieve images of the same individual from a large gallery captured across multiple camera views, given a query image. In recent years, Re-ID has achieved remarkable progress. However, despite the high accuracy achieved on a specific domain, there remains a significant gap between current Re-ID settings and real-world applications. This gap is primarily due to the fact that data distributions in practical scenarios are dynamic and continuously evolve over time, rather than remaining confined to a single domain [1]. Storing all data for joint training is often impractical in real-world deployments. This limitation has motivated the study of lifelong person re-identification (LReID), which focuses on enabling models to continuously learn across multiple domains [2]. The goal is to ensure that the model can retain strong performance on previously seen domains while adapting to new ones.

This work was supported by the Zhejiang Province Natural Science Foundation of China [Grant Z24F030004] and the National Natural Science Foundation of China [Grant 62173302]. (Corresponding author: Wei Jiang)

Mingyu Wang, Haojie Liu, Zhiyong Li, Wei Jiang are with the College of Control Science and Engineering, Zhejiang University, Hangzhou 310027, China.(e-mail: {wangmingyu, liuhaojie, lizhiyong_zju, jiangwei_zju}@zju.edu.cn)

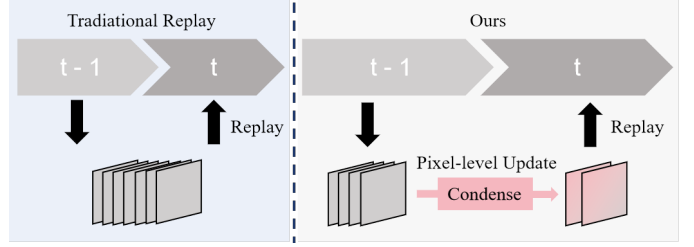


Fig. 1. Comparison of replay. Unlike previous replay-based methods that store raw images, our method condenses features from multiple samples into a single representation with pixel-level update, enhancing privacy.

A major challenge in LReID is the forgetting problem caused by domain shifts. After adapting to a new domain, the model often suffers a significant performance drop on previously learned domains. Recent literature has addressed this issue through various perspectives, including knowledge distillation [3], data replay [4], and exemplar-free distribution rehearsing methods [5]. Among these, replay-based methods store a small set of samples from previous tasks in an auxiliary memory. By replaying these samples during training on the current domain, these methods can effectively mitigate forgetting with relatively low computational cost. However, they raise concerns related to data privacy, which has led to the development of exemplar-free strategies such as distribution rehearsing. These methods train an additional network to capture the style of previous domains. During training on the current domain, these auxiliary networks are used to perform domain stylization, helping the model adapt to domain shifts. This helps reduce forgetting caused by domain shifts. However, since only domain distribution information is replayed, domain-specific styles may still be forgotten over time, resulting in performance drops on earlier domains.

To address the above challenge, we propose a novel approach that enables the replay of past features while preserving data privacy. As illustrated in Fig. 1, our method condenses features from multiple images into a single synthetic sample. This not only enriches the semantic representation of the synthesized data but also inherently enhances privacy protection, as the synthesized images undergo fine-grained pixel-level transformations. Specifically, we propose a Privacy-Preserving Replay (Pr²R) method to fuse the information from original images into a small number of synthesized samples that are both privacy-preserving and informative. After each task, we initialize synthesized samples using the clustering centers of the current domain. These samples are then updated by sequentially distilling knowledge from real images. The update process involves two key components: representativeness and privacy preservation. For representativeness, we match training

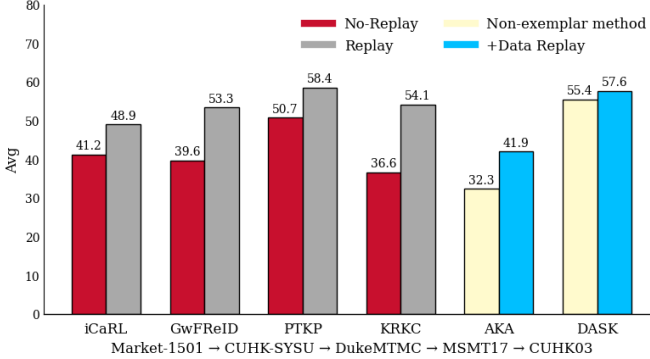


Fig. 2. Performance comparison of different methods. We observe that incorporating data replay consistently improves performance, regardless of whether the method initially relies on it, highlighting its effectiveness in LReID scenarios.

gradients between real and synthetic samples across multiple stages of the network, ensuring that synthetic data can provide similar parameter updates during replay. Additionally, an identity (ID) loss is introduced to guide the samples toward the current class. For privacy preservation, we focus on facial regions, which are more likely to raise privacy concerns. Specifically, we define a fixed rectangular region and apply Gaussian blur to this area. During image updates, samples are optimized at the global pixel level based on gradient. Leveraging both the facial mask and global pixel optimization, the samples exhibit changes in color, structure, and texture compared to the original, enhancing privacy protection. By introducing privacy-preserving data replay, we re-enable the use of replay in continual learning scenarios. As shown in Fig. 2, several existing methods avoid replay due to privacy concerns, which results in degraded performance. In contrast, our approach allows replay to be utilized effectively while ensuring data privacy.

During style replay, we mitigate cross-domain forgetting through a dual-alignment strategy. Specifically, we introduce both deep and shallow level matching constraints to guide the training of the transformation network. The trained network is then applied to current-domain features to generate hybrid samples that preserve content of the current domain while adopting previous domain styles. Conversely, we also apply it to replay samples to generate samples with old-domain content and new-domain style. These samples are jointly trained with the current data, enabling the model to retain prior knowledge while adapting to new domains.

The main contributions of this paper are as follows:

(1) We propose a new privacy-preserving data replay paradigm, Pr^2R , which performs pixel-level optimization to retain feature information from previous tasks without accessing raw data.

(2) During style replay, we adopt a dual-alignment strategy and jointly train on the transformed samples to reduce cross-domain forgetting.

(3) Extensive experiments on multiple benchmarks show that our method outperforms existing state-of-the-art approaches by up to 5% in accuracy. Notably, it achieves an average performance on seen domains that is only 6.6% lower than joint training on all domains, despite not accessing the

full data. Moreover, it outperforms joint training by 6.7% on generalization metrics, demonstrating its strong generalization capacity.

II. RELATED WORKS

A. Person Re-Identification

Person Re-Identification (Re-ID) aims to retrieve images of the same identity from a large gallery across different camera views, given a query image [6]. Extensive research has been conducted across various Re-ID settings, such as the standard image-based scenario [7], [8], video-based scenario [9], [10], and cross-modality scenario [11], [12]. While these studies often assume static datasets and rely on sufficient training time to achieve high accuracy, such settings demand significant human effort and computational resources, making them impractical for real-world applications [13]. In real-world scenarios, data continuously evolves over time, posing new challenges to Re-ID systems [14], [15]. To address this, researchers have introduced the concept of LReID [2], which focuses on continuously adapting Re-ID models to dynamically changing data distributions in a more practical way.

Recently, several privacy-preserving methods have been explored; however, most of them rely on encryption-decryption schemes [16] or user-specific keys [17], which may not be well suited for the efficiency-demanding lifelong Re-ID scenarios. To address this limitation, we propose an information-fused strategy that eliminates the need for decryption or key management, while simultaneously enhancing image representativeness and preserving privacy.

B. Lifelong Person Re-Identification

LReID [2] requires the model to continuously adapt to new domains while preserving knowledge acquired from previous ones. A major challenge in this setting is the catastrophic forgetting of prior knowledge [18]. Existing studies mainly address this issue through knowledge distillation [19], data replay [4], and distribution replay strategies [5].

Knowledge distillation [20], [21] aims to align the output distribution between the old model, which contains information from previous domains, and the new model, which is being updated with knowledge from the current domain. However, as the training progresses, the unique features of historical domains are gradually forgotten due to continual parameter updates [2], resulting in degraded performance.

Data replay strategy [4], [22] maintains a small memory buffer that stores a limited number of past samples, which are jointly trained with data from the current domain. Despite its effectiveness and low computational overhead, storing raw samples raises privacy concerns [5]. To tackle this concern, distribution replay methods [5], [23] have been introduced. Instead of storing raw samples, these approaches aim to reconstruct the feature distributions of previous domains using auxiliary networks. During training on a new domain, these auxiliary models are used to project current domain features into the style space of previous domains, mitigating domain shift and knowledge forgetting. However, since only style information is replayed, the unique semantic features of past

domains are still gradually forgotten over time. In this work, we propose a privacy-preserving data replay approach that jointly replays features and styles of previous domains.

C. Dataset Distillation

Dataset Distillation (DD) aims to condense the knowledge of large-scale datasets into significantly smaller synthetic datasets while maintaining comparable training performance.

Existing DD approaches can be categorized into several types: matching-based methods, which align training dynamics such as gradients [24], [25], feature distributions [26], or training trajectories [27]; and methods based on generative priors [28]. Pixel-level updates in DD often induce substantial semantic changes to the synthesized images, which raises growing concerns around privacy preservation. Recent efforts have emerged to explore privacy-protected dataset distillation, aiming to mitigate the risk of sensitive information leakage [29], [30]. Motivated by both dataset distillation and the challenges encountered in replay-based methods, we propose to apply pixel-level updates to fuse the information from the original images into synthetic samples, making them different from the raw data. The synthetic samples are privacy protected and semantically informative, improving replay efficiency while also enhancing data privacy and security.

III. PRELIMINARIES

A. Background on Dataset Distillation

The general goal of dataset distillation (DD) is to generate a small synthetic dataset $\mathcal{S} = \{(x_i, y_i)\}_{i=1}^{N_S}$ from a large-scale dataset $\mathcal{T} = \{(x_i, y_i)\}_{i=1}^{N_T}$, where the synthetic data retains most of the important information from the original data. Here, each x_i denotes an image with a corresponding class label y_i , and $N_S \ll N_T$.

The ultimate purpose of DD is to synthesize a small set of data that enables models trained on it to perform similarly to those trained on the full dataset. Based on this, the objective of DD can be formulated as minimizing the performance gap on the original evaluation set between models trained on the synthetic data and those trained on the full dataset:

$$\min_{\mathcal{S}} \mathbb{E}_{(x, y) \sim \mathcal{T}} [\ell(\phi_{\theta_{\mathcal{T}}}(x), y) - \ell(\phi_{\theta_{\mathcal{S}}}(x), y)], \quad (1)$$

where $\ell(\cdot, \cdot)$ and θ represent loss function and parameters of the networks, respectively. However, each time \mathcal{S} is updated, the network needs to be retrained from scratch, which leads to high computational cost. Therefore, some existing methods attempt to avoid repeated training loops by introducing surrogate objectives. In this way, the optimal synthetic dataset \mathcal{S}^* can be obtained by optimizing:

$$\mathcal{S}^* = \arg \min_{\mathcal{S}} \mathbb{E}_{\theta} [\ell(\psi(\mathcal{T}; \theta), \psi(\mathcal{S}; \theta))], \quad (2)$$

Here, ψ denotes a surrogate objective, such as gradients or distribution statistics. In this work, we adopt gradient matching as the core framework and propose a multi-stage matching strategy to update the synthetic data for LReID. This design aims to preserve data privacy while enhancing the information density of the replay data.

B. Replay-based LReID

In this work, we focus on the LReID setting. We consider a sequence of T tasks $D = \{D_t\}_{t=1}^T$, where each task $D_t = \{(x_t^i, y_t^i)\}_{i=1}^{n_t}$ contains n_t pairs of data sample and identity label. At each training step t , the model is only allowed to access the current task D_t , while previous tasks $\{D_1, \dots, D_{t-1}\}$ are no longer accessible. After training on task t , the model K_t is evaluated on a set of t test datasets $D^e = \{D_1^e, \dots, D_t^e\}$, each corresponding to a previously seen training domain. The objective of LReID is to maximize the overall identification accuracy across all tasks.

To tackle the challenge of LReID, replay-based methods maintain a small auxiliary memory $\mathcal{M} = \{(x_m, y_m)\}_{m=1}^N$ to store representative samples from previous tasks, where N denotes the memory size. As illustrated in Fig. 1, we select original samples (x_m, y_m) from the data stream and compress multiple images into a single image $(\tilde{x}_m, \tilde{y}_m)$ to construct the memory $\tilde{\mathcal{M}}$. During each iteration of the current task, a batch $\tilde{\mathcal{B}}_m = \{(\tilde{x}_m^i, \tilde{y}_m^i)\}_{i=1}^{B_m}$ is sampled from the memory and jointly trained with the current batch $\mathcal{B}_t = \{(x_t^i, y_t^i)\}_{i=1}^{B_t}$. The joint training process is formulated as follows:

$$\theta^* = \arg \min_{\theta} \mathcal{L}(\theta; \mathcal{B}_t) + \lambda \mathcal{L}_r(\theta; \tilde{\mathcal{B}}_m), \quad (3)$$

where θ denotes the parameters of the model, $\mathcal{L}(\cdot, \cdot)$ is the training objective for the current task, $\mathcal{L}_r(\cdot, \cdot)$ is the objective for data replay, and λ is a balancing coefficient. Accessing data from previous domains during training on the current domain can help mitigate the problem of cross-domain forgetting. However, as shown in Fig. 2, some existing works avoid using replay due to privacy concerns, which leads to performance degradation. To address this, we propose to condense multiple images from the data stream into a single image, enabling replay while preserving data privacy.

IV. METHOD

A. Privacy-Preserving Data Replay

The objective of this section is to synthesize privacy-preserving replay data and leverage it to construct a more informative auxiliary memory, thereby improving replay efficiency. By jointly training on the fused replay data and the current domain data, the model can better mitigate forgetting. The overall pipeline of our proposed Pr²R is illustrated in Fig. 3.

Privacy-Preserving Image Masking. To fundamentally address privacy concerns, we apply region-wise blurring to sensitive areas in the replay buffer before performing image condensation. Specifically, we target the facial regions, which are most likely to reveal identity information. Given an input image x_i , we define a fixed rectangular region of interest (ROI) and apply Gaussian blur to this area to produce a mosaic-like effect. Since the blurred samples are further optimized through pixel-level condensation, the potential loss in replay effectiveness due to blurring is largely mitigated.

Gradient-guided Data Condensation. The primary goal of the proposed Pr²R method is to enhance replay efficiency while preserving data privacy. As shown in Eq. 2, DD aims to

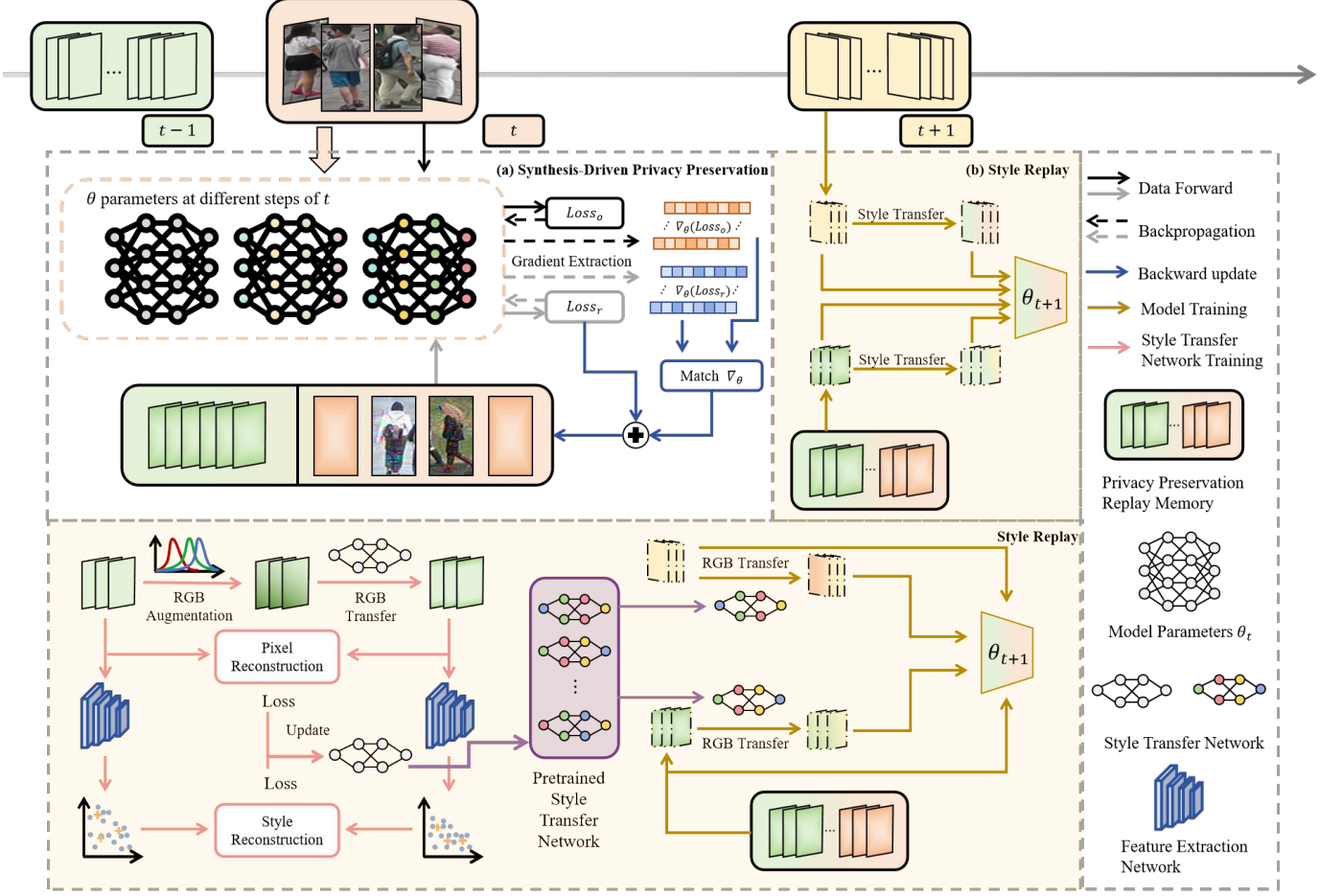


Fig. 3. Pipeline of our proposed Pr²R. Top: (a) During the training phase on domain D_t , the module stores model parameters at different time steps. It then performs pixel-level updates on replay samples by aligning their gradients with those of the original data across multiple parameters stages, generating privacy-preserving yet informative samples. (b) Leveraging the dual-alignment mechanism, the module applies style transfer to both the current domain D_{t+1} and the replay samples, effectively mitigating forgetting induced by domain shifts. Bottom: Pipeline of style model training and data replay. The left shows the style transfer network training, supervised by both pixel reconstruction and style reconstruction losses, and stored for later use. The right illustrates style replay, where style transfer is applied to both replayed and current training data, mitigating forgetting induced by domain shifts.

synthesize samples that elicit similar training responses as the full original dataset. Inspired by this insight, we adopt a multi-stage gradient matching strategy to condense the knowledge from real data into replay samples.

In the task setting, as shown in Eq. 1, we aim to generate a set of replay data \mathcal{S} such that the network parameters trained on them (θ_k^S) are similar to those trained on the original dataset (θ_k^T) at each training stage k , thereby achieving comparable performance. Based on this objective, Eq. 1 can be reformulated as:

$$\min_{\mathcal{S}} \mathbb{E}_{\theta} \left[\sum_{k=0}^{K-1} \mathcal{D}(\theta_k^S, \theta_k^T) \right] \quad (4)$$

where K denotes the total number of training steps, $\mathcal{D}(\cdot, \cdot)$ denotes the distance metric, and θ_k^S and θ_k^T refer to the model parameters at step k when trained on the replay data and the original data, respectively.

The update of θ_k^S and θ_k^T from step $k-1$ to k can be implemented as:

$$\theta_k^S \leftarrow \theta_{k-1}^S - \eta_{\theta} \nabla_{\theta} \mathcal{L}^S(\theta_{k-1}^S), \quad \theta_k^T \leftarrow \theta_{k-1}^T - \eta_{\theta} \nabla_{\theta} \mathcal{L}^T(\theta_{k-1}^T), \quad (5)$$

where η_{θ} is the learning rate. According to Eq. 4, the update can be decomposed into two parts. First, we ensure that the model parameters θ_k^S and θ_k^T are aligned at each training stage k . Based on this alignment, the second part is to match the gradients $\nabla_{\theta} \mathcal{L}^S(\theta_{k-1}^S)$ and $\nabla_{\theta} \mathcal{L}^T(\theta_{k-1}^T)$ as closely as possible.

Since θ^S and θ^T are updated from the same initialization, minimizing $D(\nabla_{\theta} \mathcal{L}^S(\theta_{k-1}^S), \nabla_{\theta} \mathcal{L}^T(\theta_{k-1}^T))$ to near zero during the update phase is sufficient to ensure that $D(\theta_k^S, \theta_k^T) \approx 0$. We can simplify the formulation in Eq. 4:

$$\min_{\mathcal{S}} \mathbb{E}_{\theta} \left[\sum_{t=0}^{T-1} \mathcal{D}(\nabla_{\theta} \mathcal{L}^S(\theta_k^S), \nabla_{\theta} \mathcal{L}^T(\theta_k^T)) \right]. \quad (6)$$

Based on the property that $D(\theta_k^S, \theta_k^T) \approx 0$ holds at each stage, we propose a more efficient matching strategy in the LReID framework. During ReID training, we store model parameters at multiple stages, forming a parameter set $\tilde{\theta}_k^T \mid t \in \mathcal{T}_s$, where \mathcal{T}_s denotes a set of selected training stages

used for gradient matching. In the gradient matching phase, we use these pre-saved parameters to represent θ_k^S and θ_k^T , which significantly improves the efficiency of gradient matching :

$$\min_S \mathbb{E}_\theta \left[\sum_{t \in \mathcal{T}_s} \mathcal{D}(\nabla_\theta \mathcal{L}^S(\tilde{\theta}_k^T), \nabla_\theta \mathcal{L}^T(\tilde{\theta}_k^T)) \right]. \quad (7)$$

ID Loss. Based on the above optimization objectives, we observe that the current design focuses solely on intra-class (same ID) optimization, without considering inter-class relationships. Traditional DD methods often overlook this issue, as they are typically applied to object-centric datasets where class differences are relatively large. However, in ReID settings, the problem involves fine-grained image recognition, and the inter-class variance is relatively small.

To address this, we introduce an **ID Loss** to keep samples aligned within their classes during updates. This helps prevent inter-class misalignment or drift, allowing the classifier to build more reliable decision boundaries and enhancing the replay effects. The identity loss is composed of two widely adopted objectives in person re-identification: a cross-entropy loss \mathcal{L}_c and a triplet loss \mathcal{L}_t . Specifically, we formulate the classification loss as follows:

$$\mathcal{L}_c = -\frac{1}{N} \sum_{i=1}^N \log \left(\frac{\exp(s_{i,y_i})}{\sum_{j=1}^C \exp(s_{i,j})} \right), \quad (8)$$

where N is the number of training samples in a mini-batch, C is the total number of identity classes, $s_{i,j}$ denotes the predicted logit for the j -th class of the i -th sample, and y_i is the ground-truth identity label for sample i . This loss encourages the network to assign higher confidence scores to the correct identity class.

We further adopt the widely used triplet loss \mathcal{L}_t [31]. Given a batch of N samples with embeddings $\{\mathbf{f}_i\}_{i=1}^N$ and labels $\{y_i\}_{i=1}^N$, for each anchor \mathbf{f}_i , we select the hardest positive and negative samples:

$$d_{ap}^{(i)} = \max_{j: y_j = y_i} \|\mathbf{f}_i - \mathbf{f}_j\|_2, \quad d_{an}^{(i)} = \min_{j: y_j \neq y_i} \|\mathbf{f}_i - \mathbf{f}_j\|_2. \quad (9)$$

The final triplet loss is computed as:

$$\mathcal{L}_t = \frac{1}{N} \sum_{i=1}^N \log \left(1 + \exp \left(d_{ap}^{(i)} - d_{an}^{(i)} \right) \right). \quad (10)$$

Finally, the overall loss \mathcal{L}_s used to update replay samples is defined as follows:

$$\mathcal{L}_s = \underbrace{\alpha \cdot \mathcal{D} \left(\nabla_\theta \mathcal{L}^S(\tilde{\theta}_k^T), \nabla_\theta \mathcal{L}^T(\tilde{\theta}_k^T) \right)}_{\text{Gradient-guided Data Condensation}} + \underbrace{\mathcal{L}_c + \mathcal{L}_t}_{\text{ID Loss}}. \quad (11)$$

Here, α is a weighting hyperparameter. Guided by \mathcal{L}_s , the samples in the replay buffer are updated at the pixel level. This not only enhances data privacy by deviating from the original ones but also leads to the generation of more informative images compared to those selected by traditional replay methods, thereby improving replay efficiency.

B. Efficient Style Replay

During the replay phase, we train the model using both current-domain samples and those stored in the replay memory. However, the replay memory often contains samples from multiple domains, and the discrepancy in domain-specific styles can hinder effective training, which has been largely overlooked by previous replay-based methods.

Inspired by Dask [5] and CoP [23], we explore the integration of style transfer into replay-based LReID frameworks to mitigate forgetting caused by domain shifts. Previous methods mainly focus on scenarios without access to replay data. In contrast, our method addresses the privacy concerns in replay-based approaches, making it possible to combine style transfer with replay methods. While prior works mainly emphasize pixel-level reconstruction, we further introduce a feature-level matching objective to capture richer representations. Specifically, we apply style transfer to both current samples and replay samples. This allows the same content to be expressed in different domain styles, facilitating better retention of cross-domain knowledge. The overall pipeline of style model training and data replay is illustrated in Fig. 3.

Given an input sample s , we first apply channel-wise style augmentation. Specifically, the augmented mean μ_r and standard deviation σ_r are computed by randomly sampling a batch from the current dataset and calculating the per-channel mean and standard deviation across the batch. This operation allows us to simulate various domain-specific style distributions within a single dataset.

For reconstruction, we follow DASK and employ the Adaptive Kernel Prediction Network (AKPNet), which comprises a lightweight CNN backbone and a linear layer. AKPNet generates a transfer kernel k for the augmented input s' , which is then used as a convolution filter to process the augmented image s' , producing the reconstructed output \hat{s} .

For style transfer, while prior methods CoP and DASK rely solely on pixel-level L1 loss, which compares images directly in the RGB space, such a constraint may limit the model's ability to capture high-level structural consistency. To address this, we incorporate a perceptual loss that measures feature-level discrepancy using a fixed, truncated VGG-16 network. Specifically, we extract intermediate features from the early layers of VGG-16, which are known to capture local texture and mid-level structural cues with minimal computational cost. Let $\xi(\cdot)$ denote the fixed (non-trainable) feature extractor:

$$\mathcal{L}_{\text{perc}} = \|\xi(\hat{s}) - \xi(s)\|_2^2 \quad (12)$$

where \hat{s} is the reconstructed image and s is the target image. This encourages the reconstructed output to not only match the target in pixel space, but also preserve structural similarity in the feature space, leading to better visual fidelity.

The overall loss is defined as a weighted combination of the L1 reconstruction loss and the proposed perceptual loss:

$$\mathcal{L}_{\text{total}} = \mathcal{L}_{\text{L1}} + \beta \cdot \mathcal{L}_{\text{perc}} \quad (13)$$

where:

- $\mathcal{L}_{\text{L1}} = \|\hat{s} - s\|_1$ ensures pixel-wise fidelity,
- $\mathcal{L}_{\text{perc}}$ enhances structure and texture consistency,

Algorithm 1 Pr²R

Input: Current task D_t , memory \mathcal{M} , replay data $\mathcal{S} \subset \mathcal{M}$
Required: Model parameters θ trained on domain $t-1$; number of update steps Z ; learning rates for LReID model weights γ, λ , and synthetic samples η_S
Initialize: Apply image masking to samples from domain t stored in memory \mathcal{M}

- 1: **for** $z = 0$ to $Z - 1$ **do**
- 2: Sample mini-batch $\mathcal{B}_t^c \sim D_t$ and $\mathcal{B}_m^c \sim \mathcal{M}$, both from class c
- 3: Calculate loss \mathcal{L}_S by Eqs. 7, 8, 10, and 11
- 4: Update synthetic samples:

$$\mathcal{S} \leftarrow \mathcal{S} - \eta_S \nabla_{\theta} \mathcal{L}_S$$

- 5: **end for**
- 6: Apply style transfer to both current domain samples and replay samples
- 7: Calculate overall loss by Eq. 14:

$$\mathcal{L} = \mathcal{L}(\theta; \mathcal{B}_t) + \gamma \mathcal{L}(\theta; \mathcal{B}'_t) + \lambda \left(\mathcal{L}_r(\theta; \tilde{\mathcal{B}}_m) + \gamma \mathcal{L}_r(\theta; \tilde{\mathcal{B}}'_m) \right)$$

- 8: Update model parameters:

$$\theta \leftarrow \theta - \nabla_{\theta} \mathcal{L} - \gamma \nabla_{\theta} \mathcal{L} - \lambda \nabla_{\theta} \mathcal{L}$$

- 9: **return** Updated model θ_t , updated privacy-preserving memory \mathcal{M}

- β balances the perceptual constraint.

By incorporating both the replay data and the style-transferred images into training, the overall objective function is reformulated as:

$$\theta^* = \arg \min_{\theta} \mathcal{L}(\theta; \mathcal{B}_t) + \gamma \mathcal{L}(\theta; \mathcal{B}'_t) + \lambda \left(\mathcal{L}_r(\theta; \tilde{\mathcal{B}}_m) + \gamma \mathcal{L}_r(\theta; \tilde{\mathcal{B}}'_m) \right) \quad (14)$$

where \mathcal{B}_t and \mathcal{B}'_t denote the current task batch before and after style transfer, respectively, and $\tilde{\mathcal{B}}_m$ and $\tilde{\mathcal{B}}'_m$ represent the replay batch before and after style transfer. γ and λ are weighting coefficients. Following prior works in LReID, the loss function \mathcal{L} and \mathcal{L}_r is composed of a Triplet Loss and a Cross-Entropy Loss, as defined in Eq. 8 and Eq. 10.

V. EXPERIMENTS

A. Benchmarks and Evaluation Metrics

Benchmarks. We conduct all experiments on the LReID benchmark, which consists of five ReID datasets: Market1501 [32], DukeMTMC [33], CUHK-SYSU [34], MSMT17-V2 [35], and CUHK03 [36]. Following previous work [2], we adopt two training orders to simulate various lifelong learning scenarios.¹ ² In addition to the training datasets, we further evaluate the model on seven unseen

¹Train Order 1: Market-1501 → CUHK-SYSU → DukeMTMC → MSMT17 → CUHK03

²Train Order 2: DukeMTMC → MSMT17 → Market-1501 → CUHK-SYSU → CUHK03

TABLE I
STATISTICS OF THE DATASETS UNDER ORIGINAL AND LREID SETTINGS.

Type	Datasets	Original Identities			LReID Identities		
		Train	Query	Gallery	Train	Query	Gallery
Replay	CUHK03	767	700	700	500	700	700
	Market-1501	751	750	751	500	751	751
	DukeMTMC	702	702	1110	500	702	1110
	CUHK-SYSU	942	2900	2900	500	2900	2900
	MSMT17	1041	3060	3060	500	3060	3060
Unseen Domains	i-LIDS	243	60	60	-	60	60
	VIPeR	316	316	316	-	316	316
	GRID	125	125	126	-	125	126
	PRID	100	100	649	-	100	649
	CUHK01	485	486	486	-	486	486
	CUHK02	1677	239	239	-	239	239
	SenseReID	1718	521	1718	-	521	1718

ReID datasets (CUHK01 [37], CUHK02 [38], VIPeR [39], PRID [40], iLIDS [41], GRID [42] and SenseReID [43]) to assess its generalization ability.

Detailed Overview of LReID Benchmarks. To ensure a fair comparison, we follow the settings proposed by [2], [5], adopting two types of LReID benchmarks. The detailed statistics are presented in Tab. I. Both benchmarks consist of 12 existing ReID datasets, differing only in the order of domain training. Here, *Original Identities* denotes the number of identities in the original datasets, while *LReID Identities* refers to the selected subset used in the LReID benchmark.

For the CUHK-SYSU dataset, we follow the preprocessing method of [2], where ground-truth person bounding box annotations are used to crop individual person images. We then select a subset in which each identity contains at least four bounding boxes. In the LReID benchmark, the number of *LReID Identities* is set to 500 for each training domain to ensure identity-balanced conditions.

Evaluation Protocol. We use mean Average Precision (mAP) and Rank-1 accuracy (R@1) on each dataset to evaluate the model's performance on specific domains. Furthermore, the average mAP and average R@1 across all training (seen) and unseen domains are calculated to evaluate the model's resistance to forgetting and its overall generalization ability in the lifelong learning setting.

B. Implementation Details

To ensure a fair comparison with previous works, we adopt ResNet-50 as the backbone of our ReID model. In contrast, the backbone of AKPNet is MobileNetV3 [44]. For sample condensation updates, a ResNet-50 network is used to extract features and compute training gradients. During the sample update stage, each sample is trained for 3 epochs. For the style replay learning phase, each dataset is trained for 50 epochs. For both training orders, the first dataset is trained for 80 epochs, while each subsequent dataset is trained for 60 epochs. All input images are resized to 256×128 and augmented with random cropping, random erasing, and horizontal flipping. We set the batch size to 128, where 32 identities are sampled with 4 images per identity. The model is optimized using SGD with a learning rate of 0.008 and a weight decay of 0.0001. The hyperparameters γ and λ are set to 4.5 and 1.0, respectively.

TABLE II

COMPARISON OF DIFFERENT METHODS ON TRAINING ORDER-1 WITH MAP AND R1 SCORES. BEST RESULTS ARE HIGHLIGHTED IN **DEEP LAVENDER** AND SECOND BEST IN **LIGHT LAVENDER**.

Method	Publication	Market-1501		CUHK-SYSU		DukeMTMC		MSMT17		CUHK03		Seen-Avg		UnSeen-Avg		
		mAP	R@1	mAP	R@1	mAP	R@1	mAP	R@1	mAP	R@1	mAP	R@1	mAP	R@1	
CIL	JointTrain	-	78.9	90.9	86.7	88.2	71.2	82.9	36.2	61.2	61.2	63.4	66.8	77.3	59.4	52.6
	LwF	TPAMI 2017	56.3	77.1	72.9	75.1	29.6	46.5	6.0	16.6	36.1	37.5	40.2	50.6	47.2	42.6
	SPD	ICCV 2019	35.6	61.2	61.7	64.0	27.5	47.1	5.2	15.5	42.2	44.3	34.4	46.4	40.4	36.6
	PRAKA	ICCV 2023	37.4	61.3	69.3	71.8	35.4	55.0	10.7	22.7	54.0	55.6	41.3	54.2	47.7	41.6
	FCS	CVPR 2024	58.3	78.5	75.1	76.2	42.6	59.8	10.2	24.3	35.3	34.9	44.3	54.7	52.1	44.2
LReID	AKA	CVPR 2021	51.2	72.0	47.5	45.1	18.7	33.1	16.4	37.6	27.7	27.6	32.3	43.1	44.3	40.4
	KRKC	AAAI 2023	60.2	83.6	84.0	86.3	58.9	76.0	24.2	51.5	43.1	44.3	54.1	68.5	59.4	53.0
	MEGE	TPAMI 2023	39.0	61.6	73.3	76.6	16.9	30.3	4.6	13.4	36.4	37.1	34.0	43.8	47.7	44.0
	ConRFL	PR 2023	59.2	78.3	82.1	84.3	45.6	61.8	12.6	30.4	51.7	53.8	50.2	61.7	57.4	52.3
	CKP	MM 2024	53.8	76.0	81.2	83.0	49.7	67.0	18.4	40.8	44.1	45.8	49.4	62.5	58.0	51.0
	LSTKC	AAAI 2024	54.7	76.0	81.1	83.4	49.4	66.2	20.0	43.2	44.7	46.5	50.0	63.1	57.0	49.9
	DASK	AAAI 2025	61.2	82.3	81.9	83.7	58.5	74.6	29.1	57.6	46.2	48.1	55.4	69.3	65.3	58.4
	Pr ² R	Ours	67.1	84.9	84.1	85.2	59.9	76.2	32.9	61.2	57.2	59.3	60.2	73.4	66.1	59.5

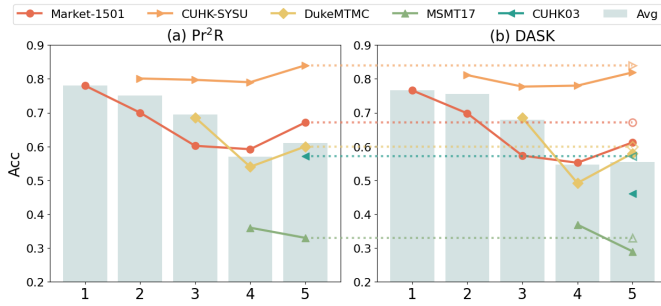


Fig. 4. Accuracy tendency on each domain and overall average trend across training stages.

For updating replay samples, we adopt SGD with a learning rate of 0.002 and a momentum of 0.9, where the coefficient α is set to 0.01. All experiments are conducted on two NVIDIA RTX 4090 GPUs.

C. Comparison with State-of-the-art Methods

We compare the proposed method with three categories of methods: (1) Class-Incremental Learning methods (CIL), including LwF [45], SPD [46], PRAKA [47] and FCS [48]; (2) Replay-based methods (KRKC [4]); and (3) Non-exemplar LReID methods (AKA [2], MEGE [19], ConRFL [49], CKP [50], LSTKC [3] and DASK [5]). In addition, we evaluate Joint Training, which leverages all available data from seen domains and serves as an upper bound for LReID methods. For fair comparison, all methods are implemented following their official publications and evaluated under the same backbone and training settings.

We first present the evaluation results on Training Order-1 and Order-2 in Tab. II and Tab. III, respectively. As we can observe, our method consistently outperforms CIL methods, replay-based LReID methods, and non-exemplar LReID methods by a clear margin. Under two training orders, it achieves average improvements of +15.2%/+17.8%, +6.5%/+6.2%, and +3.6%/+3.5% in Seen-Avg mAP/R@1 compared to the best performing methods in each respective category. Our method maintains stable performance across different training orders,

with Seen-Avg mAP/R@1 scores around 60%/73%, showing its robustness to various LReID scenarios with minimal performance fluctuations. We argue that this stability benefits from our privacy-preserving replay mechanism, which allows the model to retain both knowledge and style from previous domains, effectively mitigating forgetting. Moreover, by better preserving past knowledge, our method provides greater plasticity for learning new tasks compared to non-exemplar LReID methods, achieving an average improvement of +9.1%/+9.6% Seen-Avg mAP/R@1 improvement on CUHK03 under both training orders, demonstrating a better balance between maintaining previous performance and adapting to new tasks.

Moreover, we compare per-domain and average mAP under Training Order 1, as shown in Fig. 4. As training progresses, our method consistently outperforms state-of-the-art approaches across all domains. Notably, since all methods achieve similar performance in the initial stage, the superior performance of our method in the later stages highlights its stronger resistance to forgetting in the LReID setting. In addition, as reported in Tab. II, the observation that our method shows better plasticity on new tasks aligns with the empirical results in Fig. 4, where our method achieves a much higher mAP on CUHK03 at Stage 5. These all demonstrate that our method achieves a better balance between knowledge retention and adaptation to new information.

In terms of generalization, our method improves the Seen-Avg performance by over 5% compared to the best performing baseline, while maintaining comparable or even better performance on UnseenAvg. Furthermore, when compared to Joint Training (the performance upper bound), our method achieves an average mAP/R@1 of 63.2%/66.5%, which is similar to 63.1%/65.0% achieved by Joint Training across all twelve domains (including both seen and unseen). These results indicate that although our method involves data replay, the model does not overfit to the previously seen data. Instead, it generalizes well to unseen domains, maintaining a competitive performance. Overall, our method matches the performance of joint training in terms of average metrics across all domains,

TABLE III
COMPARISON OF DIFFERENT METHODS ON TRAINING ORDER-2 WITH MAP AND R1 SCORES.

Method	Publication	DukeMTMC		MSMT17		Market-1501		CUHK-SYSU		CUHK03		Seen-Avg		UnSeen-Avg		
		mAP	R@1	mAP	R@1	mAP	R@1	mAP	R@1	mAP	R@1	mAP	R@1	mAP	R@1	
JointTrain	-	71.2	82.9	36.2	61.2	78.9	90.9	86.7	88.2	61.2	63.4	66.8	77.3	59.4	52.6	
CII	SPD	ICCV 2019	28.5	48.5	3.7	11.5	32.3	57.4	62.1	65.0	43.0	45.2	33.9	45.5	39.8	36.3
	PRAKA	ICCV 2023	31.2	48.7	6.6	19.1	47.8	69.8	70.4	73.0	54.9	56.6	42.2	53.4	48.4	41.1
	FCS	CVPR 2024	53.6	70.0	9.5	23.5	48.7	69.9	76.2	78.2	37.1	38.4	45.0	56.0	52.7	45.1
LReID	KRK	AAAI 2023	50.1	68.6	17.7	41.1	69.0	88.3	85.2	87.4	40.4	41.6	52.5	65.4	59.4	53.4
	MEGE	TPAMI 2023	21.6	35.5	3.0	9.3	25.0	49.8	69.9	73.1	34.7	35.1	30.8	40.6	44.3	41.1
	CKP	MM 2024	49.4	67.0	14.5	33.8	56.0	77.6	83.2	84.9	45.3	47.1	49.7	62.1	57.2	50.0
	LSTKC	AAAI 2024	49.9	67.6	14.6	34.0	55.1	76.7	82.3	83.8	46.3	48.1	49.6	62.1	57.6	49.6
	DKP	CVPR 2024	53.4	70.5	14.5	33.3	60.6	81.0	83.0	84.9	45.0	46.1	51.3	63.2	59.0	51.6
	DASK	AAAI 2025	55.7	74.4	25.2	51.9	71.6	87.7	84.8	86.2	48.4	49.8	57.1	70.0	65.5	57.9
	Pr ² R	Ours	55.9	73.3	29.2	57.8	71.7	88.2	85.0	86.5	55.5	57.7	59.4	72.8	65.8	58.7

TABLE IV
ABLATION ON CONDENSE AND REPLAY COMPONENTS.

Condense	Replay		Seen-Avg		UnSeen-Avg			
	GM	ID Loss	Data R	Style R	mAP	R@1	mAP	R@1
✓			✓		54.1	69.3	57.1	52.5
	✓			✓	57.9	73.3	61.2	56.4
✓	✓			✓	55.8	71.1	58.5	54.2
✓	✓	✓		✓	58.7	72.0	62.9	57.1
✓	✓	✓	✓	✓	60.2	73.4	66.1	59.5

demonstrating a strong balance between learning efficiency and generalization.

D. Ablation Study

We show the performance comparison of the condense and replay components in Tab. IV. Here, Data R denotes the baseline with only data replay. It can be observed that progressively incorporating gradient matching and ID loss leads to notable performance improvements. Specifically, gradient matching enhances the informativeness of individual samples, thereby improving the representativeness of the replay buffer. Meanwhile, ID loss encourages the samples to retain distinctive class-discriminative features, which facilitates more reliable model predictions. Furthermore, style replay based on replay data mitigates cross-domain forgetting, while enriching each sample with multiple stylistic variations. This not only alleviates domain shift but also contributes to improved generalization performance.

VI. PARAMETER ANALYSIS

A. Condensation Parameter Analysis

We show the influence of the gradient matching weight α in Fig. 5(a). Within a proper variation range, the performance remains stable. However, further increasing the gradient matching weight on the condensed samples diminishes the consideration of inter-class relationships, leading to performance degradation. This is particularly critical in ReID tasks, where the inter-class variance is relatively small. A consistent performance drop is observed when α reaches 0.02. Based on these observations, we set α to 0.01.

B. Style Reconstruction Weight Analysis

We present the influence of the style reconstruction weight β in Fig. 5(b). It can be observed that the model performance initially improves and then degrades as the style reconstruction loss weight β increases. This is because introducing the style reconstruction loss encourages the model to better capture style-related information rather than solely focusing on pixel-level reconstruction. However, when β becomes too large, the model may overemphasize style consistency and neglect pixel-level fidelity, which undermines the realism of the transferred samples. Based on these observations, we set β to 0.01.

C. Replay Parameters Analysis

We investigate the impact of the style replay weight γ and the data replay weight λ in Fig. 5(c) and Fig. 5(d), respectively. As γ increases, the performance improves on both seen and unseen domains. This is because style replay allows the model to observe past-domain styles applied to current-domain data, as well as past data adapted to the current domain style. This enhances both forgetting resistance and style diversity during training. However, continuously increasing the weight of style replay reduces the realism of the training distribution, which negatively affects performance. We observe that the performance on seen domains starts to drop when γ exceeds 5.0.

For λ , the performance remains stable within a moderate range. However, further increasing the diversity of the replayed data leads to reduced generalization, likely because the model pays less attention to newly arriving data when overfitting to the replayed samples. A consistent performance drop is observed when λ reaches 1.5. Based on these results, we set γ to 4.5 and λ to 1.0.

VII. MODULE EFFECTIVENESS ANALYSIS

A. Privacy Analysis

We present the performance comparison after incorporating face masking and condense update in Tab. V. Specifically, we apply Gaussian blur to predefined facial regions to fundamentally address privacy concerns. As observed, introducing face masking leads to only a marginal performance drop

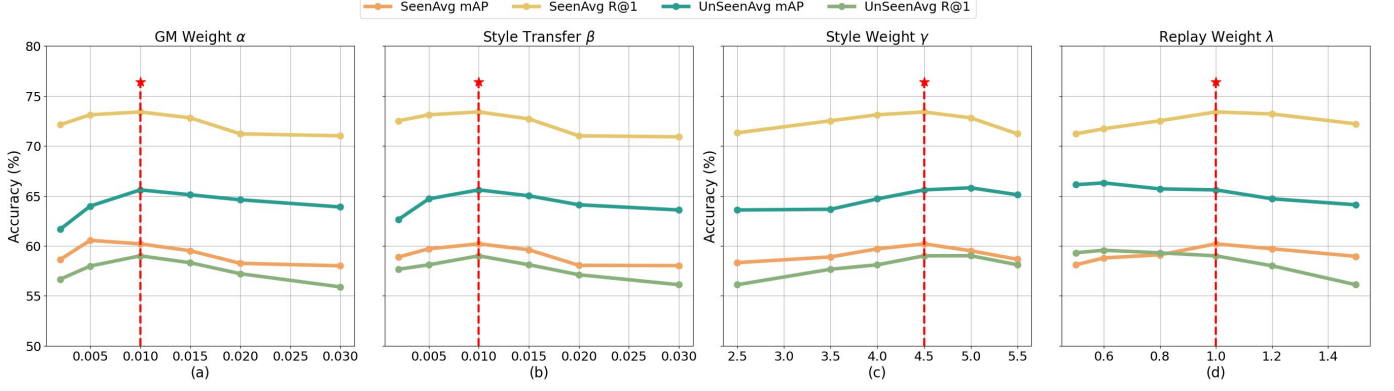


Fig. 5. Hyper-parameter analysis on (a) Gradient Match Loss Weight (Sample Update), (b) Style reconstruction loss weight in style transfer, (c) Style Replay Weight, (d) Privacy-Preserving Replay Weight. The results are obtained with our method on Training Order 1. The dashed line indicates the value adopted in this work.

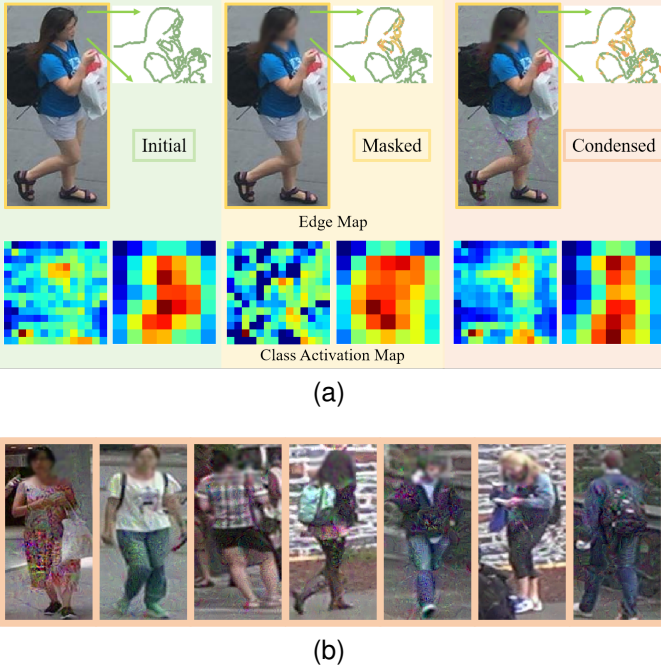


Fig. 6. Privacy analysis and visualization of condensed samples. (a) The upper part illustrates edge-detection results, where yellow regions highlight textures present in the original sample but missing in the masked and condensed image, and orange regions indicate newly added textures after the sample update. The lower part shows the CAM. As observed, the updated sample exhibits a class activation map similar to that of the original image, indicating that the masked sample is being optimized toward the correct direction. (b) The bottom image shows the samples after condensation, demonstrating that the image becomes more informative in terms of color, structure, and texture after updating, which helps improve replay performance while preserving privacy.

(1%), while generalization performance remains unaffected. As shown by the CAM in Fig.6(a), the ReID model primarily focuses on body cues. This observation aligns with [51], suggesting that ReID models rely on holistic body cues, such as clothing, posture, and body shape, rather than facial details. Therefore, obscuring the face does not impact model performance but instead reduces the risk of identity exposure, enhancing data privacy.

Furthermore, with the condense update module, samples are progressively refined towards more representative instances,

TABLE V
STUDY ON PRIVACY-PRESERVING COMPONENTS.

Condense	Replay	Mask	Seen-Avg		UnSeen-Avg	
			mAP	R@1	mAP	R@1
	✓		54.1	69.3	57.1	52.5
✓	✓		59.3	72.6	63.4	57.5
	✓	✓	52.9	68.2	57.3	52.6
✓	✓	✓	58.7	72.0	62.9	57.1

TABLE VI
PERFORMANCE COMPARISON OF DIFFERENT STRATEGIES ON THREE PERSON RE-IDENTIFICATION BENCHMARKS. EACH METHOD USES ONLY TWO SAMPLES PER CLASS.

Method	Market-1501	CUHK-SYSU	DukeMTMC
Full	78.9	86.7	71.2
Random	72.3	76.8	65.9
K-center	75.2	79.1	68.5
Pr ² R	78.8	82.5	71.0

improving replay efficiency under limited memory. Visualizations of these samples are illustrated in Edge Map in Fig.6(a) and Fig.6(b). Since gradient updates are applied at the pixel level, replay samples are optimized towards representations that align with the model's understanding while deviating from human-perceivable semantics. This improves the privacy of the replay data, as the condensed samples become less interpretable to humans yet remain effective for training. Although applying the mask leads to a slight performance drop, it is effectively compensated by the performance gain from subsequent condensation. The small sacrifice in accuracy is a worthwhile trade-off for achieving more reliable privacy protection. Our proposed masking-then-update strategy provides a practical solution to privacy concerns while further improving model performance.

B. Validation of the Condensation Mechanism

In this section, we conduct an ablation study from a different perspective to evaluate the effectiveness of our proposed condensation strategy. Specifically, we compare three sampling approaches on the Market1501 [32], CUHK-SYSU [34] and

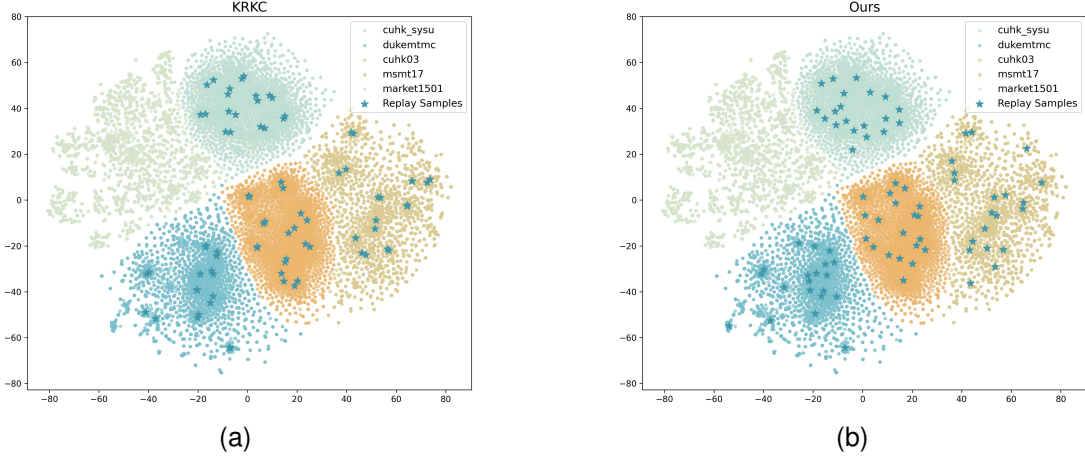


Fig. 7. Feature Distribution of Replay Samples from (a) KRKC and (b) Our method under Training Order 1.

DukeMTMC [33] benchmarks: random selection, clustering-based selection, and our condensation method. For each method, we retain two samples per class and use them to train the model.

The detailed results are presented in Tab. VI. Remarkably, our proposed Pr^2R method achieves performance comparable to training with the full dataset on both the Market-1501 and DukeMTMC benchmarks. On CUHK-SYSU, it also outperforms both the random and K-center selection strategies by a noticeable margin. This demonstrates that, under the same memory budget, our approach enables the replay buffer to preserve more diverse and informative samples, leading to improved model performance. These results highlight the efficiency of our Pr^2R strategy in utilizing limited memory for continual learning.

C. Data Replay Analysis

Most existing replay-based LReID methods adopt a unified strategy when constructing the replay memory. Specifically, they compute the mean of all features within each identity to form a “class center,” then select the top-n samples closest to this center based on feature similarity, where n is the memory size. This approach emphasizes representativeness but neglects diversity. As only a few raw images are stored, the memory space is not fully utilized.

In contrast, our method first performs clustering on the features of each identity to obtain n clusters, using each cluster center to initialize the replay memory. This ensures the representativeness of the replay samples. We then apply a multi-stage gradient matching compression strategy to condense the information of multiple samples into a single one, making each stored sample more informative and diverse.

To demonstrate the effectiveness of our approach, we visualize the t-SNE distribution of the replay samples generated by our method and the KRKC baseline during the LReID process.

As shown in Fig. 7, we visualize the t-SNE distribution of the final samples obtained by both KRKC and our proposed Pr^2R method. Compared to KRKC, our method captures more samples in high-density regions of the data sequence

while also maintains reasonable representation in low-density areas. While both methods preserve dense regions, Pr^2R achieves more comprehensive coverage across the entire data distribution. By providing a better proxy for the global data sequence, our method significantly improves model performance in LReID.

Dynamic Replay Memory. Given that different domains within the training benchmark pose varying levels of difficulty for the model, allocating an equal amount of memory to all domains is suboptimal. To address this, we adopt a dynamic replay memory strategy that adjusts memory allocation based on domain difficulty. To ensure the efficiency of replay memory construction, we employ a lightweight evaluation mechanism.

Specifically, the first domain is assigned a default memory size. For subsequent domains, memory allocation is adjusted based on the model’s performance:

- If the model achieves better performance on the current domain than its best performance on any previous domain, we reduce the memory allocated for this domain.
- Conversely, if the model performs worse on the current domain than its worst performance on any previous domain, and any prior domain had reduced memory allocation, we increase the memory allocated for the current domain.

In this work, the adjustment ratio is empirically set to 1/2. We compare our data replay module with other replay based methods [4], [22], [52]. The results are presented in Tab.VII and Tab.VIII. In this setting, we apply our proposed multi-stage gradient matching compression method to condense the samples before performing replay. Notably, no style replay is used in this comparison. It can be observed that, under the same memory budget, our method consistently outperforms previous replay-based approaches across various benchmarks. Although some methods achieve better performance on either the initial or final domains, our method demonstrates a more balanced performance overall. This can be attributed to the richer information retained in our compressed samples, enabling a better balance between past knowledge retention and new information acquisition during replay. As a result,

TABLE VII

COMPARISON OF DIFFERENT METHODS ON TRAINING ORDER-1 WITH MAP AND R1 SCORES. BEST RESULTS ARE HIGHLIGHTED IN **DEEP LAVENDER** AND SECOND BEST IN **LIGHT LAVENDER**. \dagger INDICATES RESULTS WITH DATA REPLAY ONLY, EXCLUDING STYLE REPLAY.

Method	Publication	Market-1501		CUHK-SYSU		DukeMTMC		MSMT17		CUHK03		Seen-Avg		UnSeen-Avg		
		mAP	R@1	mAP	R@1	mAP	R@1	mAP	R@1	mAP	R@1	mAP	R@1	mAP	R@1	
Replay	JointTrain	-	78.9	90.9	86.7	88.2	71.2	82.9	36.2	61.2	61.2	63.4	66.8	77.3	59.4	52.6
	GwFReID	AAAI 2021	57.7	77.4	79.6	81.7	48.5	66.4	22.0	45.0	58.8	61.4	53.3	66.4	51.4	44.9
	PTKP	AAAI 2022	73.5	88.0	84.8	86.6	59.0	75.0	23.2	47.1	51.6	53.8	58.4	70.1	57.5	51.1
	KRKC	AAAI 2023	60.2	83.6	84.0	86.3	58.9	76.0	24.2	51.5	43.1	44.3	54.1	68.5	59.4	53.0
	Pr ² R [†]	Ours	66.5	84.0	84.2	85.5	59.6	75.1	32.3	59.9	56.8	58.5	58.7	72.0	62.9	57.1

TABLE VIII

COMPARISON OF DIFFERENT METHODS ON TRAINING ORDER-2 WITH MAP AND R1 SCORES. BEST RESULTS ARE HIGHLIGHTED IN **DEEP LAVENDER** AND SECOND BEST IN **LIGHT LAVENDER**. \dagger INDICATES RESULTS WITH DATA REPLAY ONLY, EXCLUDING STYLE REPLAY.

Method	Publication	DukeMTMC		MSMT17		Market-1501		CUHK-SYSU		CUHK03		Seen-Avg		UnSeen-Avg		
		mAP	R@1	mAP	R@1	mAP	R@1	mAP	R@1	mAP	R@1	mAP	R@1	mAP	R@1	
Replay	JointTrain	-	71.2	82.9	36.2	61.2	78.9	90.9	86.7	88.2	61.2	63.4	66.8	77.3	59.4	52.6
	GwFReID	AAAI 2021	46.4	64.1	16.5	36.3	65.7	83.7	80.4	82.4	58.4	61.5	53.5	65.6	52.2	45.9
	PTKP	AAAI 2022	58.6	74.3	16.4	37.3	67.1	84.8	83.1	85.1	49.8	52.9	55.0	66.9	57.5	51.1
	KRKC	AAAI 2023	50.1	68.6	17.7	41.1	69.0	88.3	85.2	87.4	40.4	41.6	52.5	65.4	59.4	53.4
	Pr ² R [†]	Ours	55.2	72.9	28.7	56.8	70.8	87.4	84.9	86.3	55.0	57.2	58.8	72.0	63.3	56.8

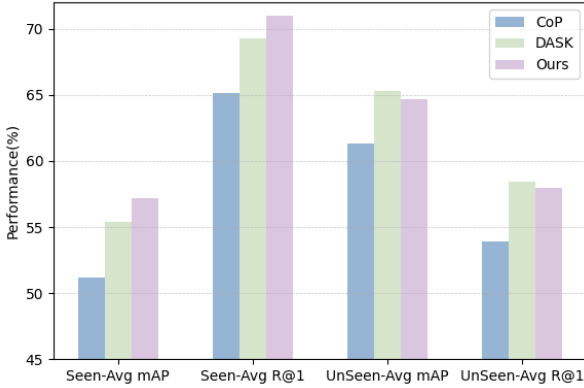


Fig. 8. Accuracy comparison under different style transfer.

our algorithm improves replay efficiency while preserving the privacy of stored samples.

D. Style Replay Analysis

In Fig. 8, we compare our proposed style transfer method with CoP and the baseline DASK. All approaches leverage past-domain style information by performing style transfer on current training data. With the introduction of a feature-level loss, our method achieves improved performance on seen domains, demonstrating its enhanced ability to replay past-domain style characteristics. This helps mitigate the forgetting issue caused by domain shifts more effectively. However, since our method places greater emphasis on modeling past-domain styles, it yields better performance on the training domain but slightly underperforms DASK in terms of generalization to unseen domains.

Impact of Style Replay on Replay Samples. During the replay phase, we train the model using both current domain samples and samples stored in the replay memory. However, the replay memory often contains samples from multiple

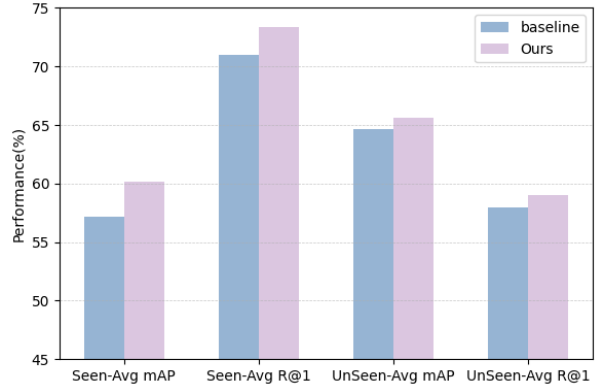


Fig. 9. Accuracy Comparison with and without Style Replay on Replay Samples.

domains, and the discrepancy in domain-specific characteristics may interfere with model training—an issue largely overlooked in previous replay-based methods. To address this, we apply style transfer to both the current-domain samples and the replay samples.

By aligning the style of replay samples with that of the current domain, the model is exposed to the same individual with varied domain-specific appearances. This helps mitigate the adverse effect of domain shifts, thus alleviating forgetting. We demonstrate the effectiveness of our proposed module in Fig. 9. Specifically, the baseline involves applying style transfer only to current-domain training data, while the replay samples remain unaltered. In contrast, our approach applies style transfer to both current and replay samples, leading to improved performance and better resistance to domain shifts.

We observe that applying style transfer to the replay samples brings consistent improvements across all evaluation metrics. This supports our hypothesis that domain discrepancies in replay data can negatively impact model training. By align-

ing features from different domains to the current domain, we improve the effectiveness of replay and enhance model performance.

VIII. CONCLUSION

In this work, we addressed the challenge of LReID and proposed a novel perspective by introducing Privacy-Preserving Data Replay (Pr²R) based on information fusion and style awareness. To the best of our knowledge, this is the first attempt to explore privacy-preserving for data replay in continual learning scenarios. Specifically, we first applied a masking strategy to the replay samples, fundamentally resolving facial privacy concerns. We then introduced data condensation to further enhance the overall privacy, not limited to facial regions, while simultaneously improving the representativeness of the replayed samples. With both privacy-preserving and more informative replay samples, our method significantly improved the replay module. Moreover, benefiting from the resolved privacy issues, we enabled the integration of style replay into data replay. By jointly applying a dual-alignment strategy to both current and replayed samples, our method effectively mitigated class-incremental challenges and forgetting caused by domain shifts. By combining these two modules, our Pr²R achieved state-of-the-art performance across various training orders, demonstrating its effectiveness and generalizability in LReID.

Furthermore, our method can be further optimized to make the fused samples more representative, which in turn improves replay efficiency. By fundamentally addressing the privacy concerns associated with previous replay-based LReID methods, our approach opens up new possibilities for more practical applications for reply-based LReID method. We hope that Pr²R can serve as a strong baseline and inspire future research in two key directions: (1) exploring the integration of information fusion with LReID, and (2) developing privacy-aware replay methods for continual learning.

REFERENCES

- [1] J. Jia, H. Xie, Q. Huang, Y. Song, and P. Wu, “Diversereid: Towards generalizable person re-identification via dynamic style hallucination and decoupled domain experts,” *Neural Networks*, vol. 189, p. 107602, 2025.
- [2] N. Pu, W. Chen, Y. Liu, E. M. Bakker, and M. S. Lew, “Lifelong person re-identification via adaptive knowledge accumulation,” in *2021 IEEE/CVF Conference on Computer Vision and Pattern Recognition (CVPR)*, 2021, pp. 7897–7906.
- [3] K. Xu, X. Zou, and J. Zhou, “Lstkc: Long short-term knowledge consolidation for lifelong person re-identification,” *Proceedings of the AAAI Conference on Artificial Intelligence*, vol. 38, no. 14, pp. 16 202–16 210, Mar. 2024.
- [4] C. Yu, Y. Shi, Z. Liu, S. Gao, and J. Wang, “Lifelong person re-identification via knowledge refreshing and consolidation,” *Proceedings of the AAAI Conference on Artificial Intelligence*, vol. 37, no. 3, pp. 3295–3303, Jun. 2023.
- [5] K. Xu, C. Jiang, P. Xiong, Y. Peng, and J. Zhou, “Dask: Distribution rehearsing via adaptive style kernel learning for exemplar-free lifelong person re-identification,” *Proceedings of the AAAI Conference on Artificial Intelligence*, vol. 39, no. 9, pp. 8915–8923, Apr. 2025.
- [6] M. Ye, J. Shen, G. Lin, T. Xiang, L. Shao, and S. C. H. Hoi, “Deep learning for person re-identification: A survey and outlook,” *IEEE Transactions on Pattern Analysis and Machine Intelligence*, vol. 44, no. 6, pp. 2872–2893, 2022.
- [7] H. Luo, W. Jiang, Y. Gu, F. Liu, X. Liao, S. Lai, and J. Gu, “A strong baseline and batch normalization neck for deep person re-identification,” *IEEE Transactions on Multimedia*, vol. 22, no. 10, pp. 2597–2609, 2020.
- [8] M. Ye and P. C. Yuen, “Purifynet: A robust person re-identification model with noisy labels,” *IEEE Transactions on Information Forensics and Security*, vol. 15, pp. 2655–2666, 2020.
- [9] S. Li, J. Leng, C. Kuang, M. Tan, and X. Gao, “Video-level language-driven video-based visible-infrared person re-identification,” *IEEE Transactions on Information Forensics and Security*, vol. 20, pp. 5505–5520, 2025.
- [10] X. Zhang, R. Han, L. Wang, L. Song, J. Hou, and W. Feng, “Synthetic-to-real video person re-id,” *IEEE Transactions on Information Forensics and Security*, vol. 20, pp. 5438–5450, 2025.
- [11] Y. Du, C. Lei, Z. Zhao, Y. Dong, and F. Su, “Video-based visible-infrared person re-identification with auxiliary samples,” *IEEE Transactions on Information Forensics and Security*, vol. 19, pp. 1313–1325, 2024.
- [12] Y. Yang, W. Hu, and H. Hu, “Progressive cross-modal association learning for unsupervised visible-infrared person re-identification,” *IEEE Transactions on Information Forensics and Security*, vol. 20, pp. 1290–1304, 2025.
- [13] J. Sun, Y. Li, L. Chen, H. Chen, and M. Wang, “Dualistic disentangled meta-learning model for generalizable person re-identification,” *IEEE Transactions on Information Forensics and Security*, vol. 20, pp. 1106–1118, 2025.
- [14] G. C. Bertocco, F. Andaló, and A. Rocha, “Unsupervised and self-adaptive techniques for cross-domain person re-identification,” *IEEE Transactions on Information Forensics and Security*, vol. 16, pp. 4419–4434, 2021.
- [15] J. Gu, W. Chen, H. Luo, F. Wang, H. Li, W. Jiang, and W. Mao, “Multi-view evolutionary training for unsupervised domain adaptive person re-identification,” *IEEE Transactions on Information Forensics and Security*, vol. 17, pp. 344–356, 2022.
- [16] M. Ye, W. Shen, J. Zhang, Y. Yang, and B. Du, “Securereid: Privacy-preserving anonymization for person re-identification,” *IEEE Transactions on Information Forensics and Security*, vol. 19, pp. 2840–2853, 2024.
- [17] G. Mai, K. Cao, X. Lan, and P. C. Yuen, “Secureface: Face template protection,” *IEEE Transactions on Information Forensics and Security*, vol. 16, pp. 262–277, 2021.
- [18] Z. Liu, C. Feng, S. Chen, and J. Hu, “Knowledge-preserving continual person re-identification using graph attention network,” *Neural Networks*, vol. 161, pp. 105–115, 2023.
- [19] N. Pu, Z. Zhong, N. Sebe, and M. S. Lew, “A memorizing and generalizing framework for lifelong person re-identification,” *IEEE Transactions on Pattern Analysis and Machine Intelligence*, vol. 45, no. 11, pp. 13 567–13 585, 2023.
- [20] Z. Cui, J. Zhou, X. Wang, M. Zhu, and Y. Peng, “Learning continual compatible representation for re-indexing free lifelong person re-identification,” in *2024 IEEE/CVF Conference on Computer Vision and Pattern Recognition (CVPR)*, 2024, pp. 16 614–16 623.
- [21] Z. Sun and Y. MU, “Patch-based knowledge distillation for lifelong person re-identification,” in *Proceedings of the 30th ACM International Conference on Multimedia*, 2022, p. 696–707.
- [22] W. Ge, J. Du, A. Wu, Y. Xian, K. Yan, F. Huang, and W.-S. Zheng, “Lifelong person re-identification by pseudo task knowledge preservation,” *Proceedings of the AAAI Conference on Artificial Intelligence*, vol. 36, no. 1, pp. 688–696, Jun. 2022.
- [23] J. Gu, H. Luo, K. Wang, W. Jiang, Y. You, and J. Zhao, “Color prompting for data-free continual unsupervised domain adaptive person re-identification,” 2023.
- [24] J. Zhang, Z. Chen, L. Dai, P. Li, and B. Sheng, “Gradient amplification for gradient matching based dataset distillation,” *Neural Networks*, vol. 191, p. 107819, 2025.
- [25] S. Vahidian, M. Wang, J. Gu, V. Kungurtsev, W. Jiang, and Y. Chen, “Group distributionally robust dataset distillation with risk minimization,” in *International Conference on Learning Representations*, 2025.
- [26] B. Zhao and H. Bilen, “Dataset condensation with distribution matching,” in *2023 IEEE/CVF Winter Conference on Applications of Computer Vision (WACV)*, 2023, pp. 6503–6512.
- [27] G. Li, R. Togo, T. Ogawa, and M. Haseyama, “Importance-aware adaptive dataset distillation,” *Neural Networks*, vol. 172, p. 106154, 2024.
- [28] J. Gu, S. Vahidian, V. Kungurtsev, H. Wang, W. Jiang, Y. You, and Y. Chen, “Efficient dataset distillation via minimax diffusion,” in *2024 IEEE/CVF Conference on Computer Vision and Pattern Recognition (CVPR)*, 2024, pp. 15 793–15 803.

[29] T. Dong, B. Zhao, and L. Lyu, “Privacy for free: How does dataset condensation help privacy?” in *Proceedings of the 39th International Conference on Machine Learning*, vol. 162. PMLR, 17–23 Jul 2022, pp. 5378–5396.

[30] D. Chen, R. Kerkouche, and M. Fritz, “Private set generation with discriminative information,” in *Advances in Neural Information Processing Systems*, vol. 35, 2022, pp. 14 678–14 690.

[31] S. He, H. Luo, P. Wang, F. Wang, H. Li, and W. Jiang, “Transreid: Transformer-based object re-identification,” in *2021 IEEE/CVF International Conference on Computer Vision (ICCV)*, 2021, pp. 14 993–15 002.

[32] L. Zheng, L. Shen, L. Tian, S. Wang, J. Wang, and Q. Tian, “Scalable person re-identification: A benchmark,” in *2015 IEEE International Conference on Computer Vision (ICCV)*, 2015, pp. 1116–1124.

[33] E. Ristani, F. Solera, R. Zou, R. Cucchiara, and C. Tomasi, “Performance measures and a data set for multi-target, multi-camera tracking,” in *Computer Vision – ECCV 2016 Workshops*. Springer International Publishing, 2016, pp. 17–35.

[34] T. Xiao, S. Li, B. Wang, L. Lin, and X. Wang, “End-to-end deep learning for person search,” *arXiv preprint arXiv:1604.01850*, vol. abs/1604.01850, 2016.

[35] L. Wei, S. Zhang, W. Gao, and Q. Tian, “Person transfer gan to bridge domain gap for person re-identification,” in *2018 IEEE/CVF Conference on Computer Vision and Pattern Recognition*, 2018, pp. 79–88.

[36] W. Li, R. Zhao, T. Xiao, and X. Wang, “Deepreid: Deep filter pairing neural network for person re-identification,” in *2014 IEEE Conference on Computer Vision and Pattern Recognition*, 2014, pp. 152–159.

[37] W. Li, R. Zhao, and X. Wang, “Human reidentification with transferred metric learning,” in *Computer Vision – ACCV 2012*, K. M. Lee, Y. Matsushita, J. M. Rehg, and Z. Hu, Eds. Springer Berlin Heidelberg, 2013, pp. 31–44.

[38] W. Li and X. Wang, “Locally aligned feature transforms across views,” in *2013 IEEE Conference on Computer Vision and Pattern Recognition*, 2013, pp. 3594–3601.

[39] D. Gray and H. Tao, “Viewpoint invariant pedestrian recognition with an ensemble of localized features,” in *Computer Vision – ECCV 2008*. Springer Berlin Heidelberg, 2008, pp. 262–275.

[40] M. Hirzer, C. Beleznai, P. M. Roth, and H. Bischof, “Person re-identification by descriptive and discriminative classification,” in *Image Analysis*. Springer Berlin Heidelberg, 2011, pp. 91–102.

[41] T. Wang, S. Gong, X. Zhu, and S. Wang, “Person re-identification by video ranking,” in *Computer Vision – ECCV 2014*. Springer International Publishing, 2014, pp. 688–703.

[42] C. C. Loy, T. Xiang, and S. Gong, “Multi-camera activity correlation analysis,” in *2009 IEEE Conference on Computer Vision and Pattern Recognition*, 2009, pp. 1988–1995.

[43] H. Zhao, M. Tian, S. Sun, J. Shao, J. Yan, S. Yi, X. Wang, and X. Tang, “Spindle net: Person re-identification with human body region guided feature decomposition and fusion,” in *2017 IEEE Conference on Computer Vision and Pattern Recognition (CVPR)*, 2017, pp. 907–915.

[44] A. Howard, M. Sandler, B. Chen, W. Wang, L.-C. Chen, M. Tan, G. Chu, V. Vasudevan, Y. Zhu, R. Pang, H. Adam, and Q. Le, “Searching for mobilenetv3,” in *2019 IEEE/CVF International Conference on Computer Vision (ICCV)*, 2019, pp. 1314–1324.

[45] Z. Li and D. Hoiem, “Learning without forgetting,” *IEEE Transactions on Pattern Analysis and Machine Intelligence*, vol. 40, no. 12, pp. 2935–2947, 2018.

[46] F. Tung and G. Mori, “Similarity-preserving knowledge distillation,” in *2019 IEEE/CVF International Conference on Computer Vision (ICCV)*, 2019, pp. 1365–1374.

[47] W. Shi and M. Ye, “Prototype reminiscence and augmented asymmetric knowledge aggregation for non-exemplar class-incremental learning,” in *2023 IEEE/CVF International Conference on Computer Vision (ICCV)*, 2023, pp. 1772–1781.

[48] Q. Li, Y. Peng, and J. Zhou, “Fcs: Feature calibration and separation for non-exemplar class incremental learning,” in *2024 IEEE/CVF Conference on Computer Vision and Pattern Recognition (CVPR)*, 2024, pp. 28 495–28 504.

[49] J. Huang, X. Yu, D. An, Y. Wei, X. Bai, J. Zheng, C. Wang, and J. Zhou, “Learning consistent region features for lifelong person re-identification,” *Pattern Recognition*, vol. 144, p. 109837, 2023.

[50] K. Xu, H. Zhang, Y. Li, Y. Peng, and J. Zhou, “Mitigate catastrophic remembering via continual knowledge purification for noisy lifelong person re-identification,” in *Proceedings of the 32nd ACM International Conference on Multimedia*, ser. MM ’24. Association for Computing Machinery, 2024, p. 5790–5799.

[51] J. Dietlmeier, J. Antony, K. McGuinness, and N. E. O’Connor, “How important are faces for person re-identification?” in *2020 25th International Conference on Pattern Recognition (ICPR)*, 2021, pp. 6912–6919.

[52] G. Wu and S. Gong, “Generalising without forgetting for lifelong person re-identification,” *Proceedings of the AAAI Conference on Artificial Intelligence*, vol. 35, no. 4, pp. 2889–2897, May 2021.